Sensitivity of Nozzle Guide Vane Flow Capacity to Geometric Changes

Tom Franklyn Gammage

June 2021

Thanks

Abstract

Contents

List of Figures

List of Tables

Nomenclature

Romans

Greeks

Acronyms and Abbreviations

Subscripts

Chapter 1

Introduction

1.1 Motivation

Jet engines are not perfect. Contemporary analysis does not provide a complete understanding of the phenomena by which turbomachinery flows differ from 1-dimensional compressible flow. Contemporary engineering does not provide a realisation of the best performing engine that could be built, but is instead limited by the capabilities of technology. It will be shown that our analytical needs and our performance needs are tied together by our need to predict the engine core mass flow rate as accurately as possible.

The requirement for an accurate core mass flow rate prediction is illustrated by consideration of the Brayton thermodynamic cycle, which is plotted in Figure 1.1.

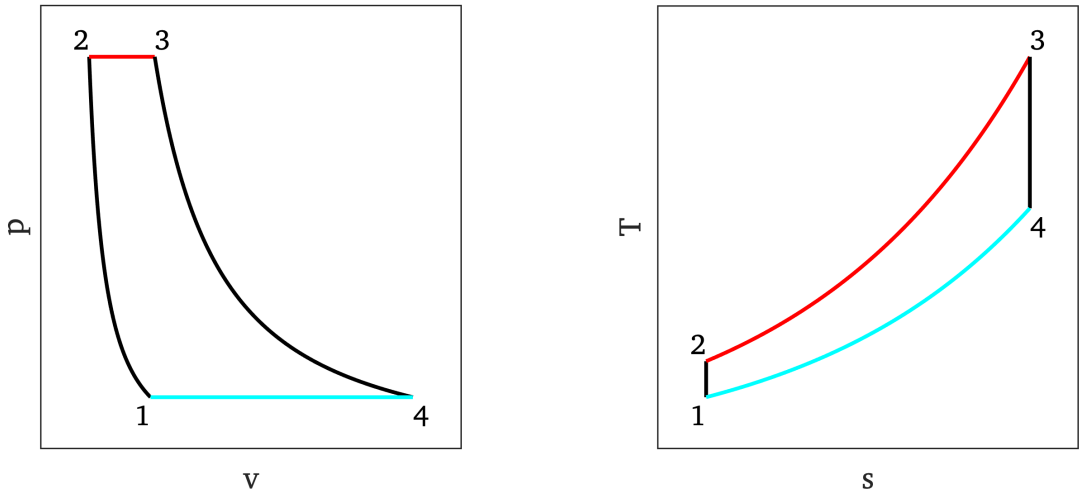

(a) p-v plot

(b) T-s plot

Figure 1.1: p-v and T-s plots of the Brayton thermodynamic cycle

Basic analysis of the Brayton cycle shows that its thermal efficiency is equal to

$$\eta_{th} = 1 - \left(\frac{p_1}{p_2}\right)^{\frac{\gamma-1}{\gamma}} \tag{1.1}$$

For maximum thermal efficiency, it is thus desirable to maximise the pressure increase produced by the engine's compressor, which is responsible for the process of isentropic compression between stations 1 and 2. The compression ratio is limited in practice by the pressure increase that is achievable by contemporary compressors, which must balance the goal with the avoidance of stall, the need for a wide range of operating conditions, and the avoidance of excess complexity from adding additional spools. Cruise-condition compression ratio is thus a design specification which sets the value of p_2.

The engine's combustor is responsible for the process of isobaric heat addition between stations 2 and 3. The rate of heat addition to the flow is given by

$$Q_{23} = \dot{m} c_p \left(T_3 - T_2\right) \tag{1.2}$$

where $\dot{m}$ is the mass flow rate through the combustor. For the purpose of illustration, the influences of bleed and cooling air mass flow rate are not considered, and $\dot{m}$ is taken to be the mass flow rate through the engine compressor, combustor, nozzle guide vanes, and turbine. c_p is the specific heat of air at constant pressure and T_2 is derived from the compressor inlet temperature T_1 via isentropic compression as

$$T_2 = T_1 \left(\frac{p_2}{p_1}\right)^{\frac{\gamma-1}{\gamma}} \tag{1.3}$$

combining to express the heat added as

$$Q_{23} = \dot{m} c_p \left[T_3 - T_1 \left(\frac{p_2}{p_1}\right)^{\frac{\gamma-1}{\gamma}}\right] \tag{1.4}$$

For maximum power, it is desirable to maximise the heat added to the flow, which would result in an increase in in T_3. A technological limitation is once again presented: the maximum T_3 is limited by the avoidance of overheating the post-combustor nozzle guide vanes, for which heat management is of prime concern to the field. T_3 is thus a design specification.

Heat addition is well controlled for in contempoary lean-burn engines, where it may be modelled by the relationship

$$Q_{23} = \eta_h H_{LV} \dot{m}_f \tag{1.5}$$

where $\dot{m}_f$ is the fuel mass flow rate, H_{LV} is the lower heating value of jet fuel and η_h is a constant to account for inefficiencies of heat addition beyond the scope of the present illustration. The above equations combine to show that the required fuel mass flow rate may be modelled by the expression

$$\frac{\dot{m}_f}{\dot{m}} = \frac{c_p}{\eta_h H_{LV}} \left(T_3 - T_1 r_p^{\frac{\gamma-1}{\gamma}}\right) \tag{1.6}$$

where r_p is the compression ratio, $\frac{p_2}{p_1}$. It is shown that the core mass flow rate, $\dot{m}$, must be accurately predicted if the engine is to be accurately maintained at the optimal operating conditions allowed by its construction. r_p and T_3 are known design specifications, T_1 is a measurable ambient condition, and all other terms are approximately constant.

The design of any jet engine depends on the assumption that accurate prediction of $\dot{m}$ is possible. It has been shown that this is directly tied to the performance and operational margins of the upstream engine components. Predictability of $\dot{m}$ also affects the design of every downstream turbine stage. If it differs from its expected value due to a poor prediction, all subsequent turbine stages will be sized for an incorrect mass flow rate. The resulting errors in flow velocity and pressure will compound with each additional stage, leading to increasingly incorrect specification of turbine sizes and turning angles.

Andrea Guiffre' and Matteo Pini [1] performed numerical analysis to discuss scaleable guidelines for turbine stage design, validating their model using high-fidelity CFD. Correct stage matching was found to be highly dependent on matching the *volumetric flow ratio*, defined by the authors as a stage's total-to-static density ratio. To accurately quantify this parameter within the analytical and computational methods discussed in this thesis, mass flow rate would need to be predicted correctly.

A strong understanding of NGV mass flow rate predictability should allow engine-makers to pre-empt geometric changes that happen to NGVs during service, such as erosion and cooling hole blockage. It should also account for geometric uncertainties arising from the manufacturing process. While this study advocates for improved accuracy of capacity predictions, emphasis is placed on how these predictions are limited by the unpredictability of real-world manufacture and service.

Section 1.2 will outline the analysis involved in parameterising and predicting mass flow rate. The section will also present the alternative metric of *flow capacity* as a more useful way of characterising mass flow rate independently of the NGV upstream total pressure and temperature. Defining a purely geometric mass flow rate capacity allows for experimental testing of NGVs without recreating the extreme boundary conditions to which real NGVs are exposed. Setting the correct pressure ratio is sufficent, as the subsequent derivation will show. This expedites the testing of different NGV geometries' effects on mass flow rate.

1.2 Flow capacity: background, definition, and derivation

The capacity of an internal combustion engine is an intuitive concept. It is simple to derive from the engine's geometry, it has tangible units of volume, and it provides an heuristic for the engine's size, performance, and air mass flow rate. The design of turbomachinery invites an analagous concept to that of IC engine capacity, but a definition is not so obvious. Mass flow rate through an engine's nozzle guide vane is a function of the NGV's geometry and of its boundary conditions. If the mass flow rate can be quantified in a way which mitigates the boundary conditions, then the effects of an NGV's geometry on its mass flow rate may be isolated. A particular NGV will thus have a mass flow rate capacity, just as a particular IC cylinder has a volumetric capacity.

In 1 dimension, an engine nozzle may be modelled as a compressible flow from an upstream reservoir of total pressure p_0, accelerating to velocity v and density ρ through a nozzle of cross-sectional area A. Mass flow rate through the nozzle is thus

$$\dot{m} = \rho A v \tag{1.7}$$

where density may be expressed as a function of *pressure ratio*, the ratio of the nozzle pressure to the total pressure

$$\rho = \frac{p_0}{RT_0}\left(\frac{p}{p_0}\right)^{\frac{1}{\gamma}} \tag{1.8}$$

and velocity is given by the compresssible form of Bernouilli's equation as

$$v = \sqrt{2\left(\frac{\gamma}{\gamma-1}\right)\left[\frac{p_0}{\rho_0} - \frac{p}{\rho}\right]} \tag{1.9}$$

The above equations combine to express mass flow rate through the nozzle as

$$\dot{m} = A\frac{p_0}{RT_0}\left(\frac{p}{p_0}\right)^{\frac{1}{\gamma}}\sqrt{2\left(\frac{\gamma}{\gamma-1}\right)\left[\frac{p_0}{\left(\frac{p_0}{RT_0}\right)} - \frac{p}{\left(\frac{p_0}{RT_0}\right)\left(\frac{p}{p_0}\right)^{\frac{1}{\gamma}}}\right]} \tag{1.10}$$

which simplifies to

$$\dot{m} = A\frac{p_0}{RT_0}\left(\frac{p}{p_0}\right)^{\frac{1}{\gamma}}\sqrt{2\left(\frac{\gamma}{\gamma-1}\right)\left[RT_0 - RT_0\left(\frac{p}{p_0}\right)^{\frac{\gamma-1}{\gamma}}\right]} \tag{1.11}$$

$$\dot{m} = \frac{p_0}{\sqrt{T_0}}A\sqrt{\frac{\gamma}{R}}\left(\frac{p}{p_0}\right)^{\frac{1}{\gamma}}\sqrt{\left(\frac{2}{\gamma-1}\right)\left[1-\left(\frac{p}{p_0}\right)^{\frac{\gamma-1}{\gamma}}\right]} \tag{1.12}$$

Using $\dot{m}$ from Equation 1.12, capacity is defined as

$$\Gamma = \frac{\sqrt{T_0}}{p_0}\dot{m} \tag{1.13}$$

This provides an expression of mass flow rate independent of upstream total pressure p_0 and upstream total temperature T_0. The expression is purely a function of throat area A and pressure ratio $\frac{p}{p_0}$:

$$\Gamma = A\sqrt{\frac{\gamma}{R}}\left(\frac{p}{p_0}\right)^{\frac{1}{\gamma}}\sqrt{\left(\frac{2}{\gamma-1}\right)\left[1-\left(\frac{p}{p_0}\right)^{\frac{\gamma-1}{\gamma}}\right]} \tag{1.14}$$

A scale constant σ is defined as

$$\sigma = \sqrt{\frac{2\gamma}{R(\gamma-1)}} \tag{1.15}$$

for a compact expression of capacity as a function of throat area A and pressure ratio r:

$$\Gamma(A,r) = \sigma A\sqrt{r^{\frac{2}{\gamma}}\left(1-r^{\frac{\gamma-1}{\gamma}}\right)} \tag{1.16}$$

This expression has its maximum value at the critical pressure ratio

$$r_c = \left(\frac{\gamma+1}{2}\right)^{\frac{\gamma}{1-\gamma}} \tag{1.17}$$

At lower ratios, the nozzle is choked and mass flow rate cannot increase further. Choked capacity is given by

$$\Gamma_c(A) = \sqrt{\frac{2\gamma}{R(\gamma-1)}}A\sqrt{\left(\frac{\gamma+1}{2}\right)^{\frac{2}{1-\gamma}}\left[1-\left(\frac{\gamma+1}{2}\right)^{-1}\right]} \tag{1.18}$$

which simplifies to

$$\Gamma_c(A) = \sqrt{\frac{2\gamma}{R(\gamma-1)}}A\sqrt{\left(\frac{\gamma+1}{2}\right)^{\frac{2}{1-\gamma}}\left[\frac{\gamma+1}{\gamma+1}-\left(\frac{2}{\gamma+1}\right)\right]} \tag{1.19}$$

$$\Gamma_c(A) = A\sqrt{\frac{2\gamma}{R}(\gamma+1)^{\frac{2}{1-\gamma}}\frac{1}{\gamma+1}\left(\frac{1}{2}\right)^{\frac{2}{1-\gamma}}} \tag{1.20}$$

$$\Gamma_c(A) = A\sqrt{\frac{\gamma}{R}}\left(\frac{\gamma+1}{2}\right)^{\frac{1+\gamma}{2(1-\gamma)}} \tag{1.21}$$

It is shown that the capacity of one-dimensional nozzle flow is a function of only the flow's minimum area, provided the flow is choked and the ratio of specific heats is assumed constant.

Section 1.3 will introduce the structure of the following chapters, which are to analyse the capacity of 2-dimensional and 3-dimensional nozzle flows, presenting and discussing analytical techniques for applying the 1D capacity equation to 2D and 3D data. In such cases, capacity will be defined by equation 1.13.

1.3 Research structure

The present study seeks to categorise and examine the ways in which nozzle guide vane flow departs from 1-dimensional compressible flow. These departures are numerous and diverse. The study's scope is to include 2 categories of phenomena: difficulties in predicting the mass flow rate through real nozzle guide vanes, and difficulties in quantifying and modelling the loss incurred by various practical solutions to the need for NGV coolant flow.

Although NGV flow capacity is arguably to be maximised in pursuit of greater power, and loss is certainly to be minimised in pursuit of greater efficiency, it is practical to divide efforts according to the areas of NGV engineering where limitations are present. The present study has identified 3 such areas.

- NGV casting processes causing variations in overall shape and throat area, limiting the predictability of flow capacity.
- Trailing edge machining processes causing variations in trailing edge shape, resulting in complex variations in the flow field near the trailing edge flange, with corresponding variations in flow capacity.
- Sensitivity of flow capacity to the addition of extra film cooling holes on the NGV leading edge suction side, including sensitivity to their exact location.

NGVs are cast to high precision. Chapter 2 will present the variations that nonetheless exist among sets of vanes that are intended to be identical. These variations are shown to affect the NGVs' geometric throat area. The chapter discusses the challenges inherent in finding a definition of throat area that usefuly predicts the flow capacity of an NGV. The effects of 2-dimensional flow phenomena and geometric variations are presented as confounding factors when considering 2D nozzle flow as opposed to 1D. Further complexity is shown to arise when extending analyses to 3D, where 3D CFD data gathered by Rolls-Royce plc are compared to 2D CFD data from the present study.

Chapter 3 will discuss the other way in which NGV manufacturing introduces geometric variations that reduce capacity predictability, namely the machining of the trailing edge shape. The machining is designed to optimise the trailing edge's aerodynamics, and not necessarily to minimise variations in its shape. The chapter presents 2D CFD analyses of the effects of variable traling edge flange size on the 2D flow field and resulting flow capacity of the NGV. To address the variability of contemporary trailing edge designs and to examine the possibility of thicker trailing edges in the event of novel manufacturing methods, the chapter presents 2D CFD analyses of a flange-less design. This design's loss performance is analysed, informed by a review of various definitions of loss from the literature, where a lack of concensus on a loss definition is demonstrated.

Chapter 4 will analyse the effects of film coolant injection location on both flow capacity and loss. The chapter discusses the possible requirement for an additional suction-side film cooling hole row to be added to NGVs. Given the variability inherent in the process of drilling film cooling holes, justification is given for a 2D CFD study of the effects of hole location on flow capacity and loss, analagous to the variable trailing edge study of Chapter 3. A correlation between hole location and flow capacity is analysed, as is the hole location's effect on loss. The chapter also presents a quasi-3D CFD study to demonstrate that 2D CFD (which amounts to a cooling slot) does not accurately model the discharge and mixing phenomena of a row of circular holes.

Literature review will not be the subject of its own chapter. Literature will be reviewed throughout the thesis whenever relevant to the topic under discussion.

1.4 Summary of findings

Write this after you've got the findings.

Chapter 2

Geometric throat area

A 1-dimensional supersonic nozzle is equivalent to a single streamline of variable cross-sectional area. It is possible to solve for the flow conditions throughout the nozzle, provided area is specified as a function of position along the nozzle. The mass flow rate capacity is a function of only the flow's minimum area, as in equation 1.21.

A 2-dimensional nozzle may be modelled as a group of adjacent streamlines, each of which may have dissimilar area functions. The streamlines' minimum areas may not correspond to a straight line across the narrowest part of the nozzle.

This is illustrated in Figure 2.1a by supposing the division of a 2-dimensional flow into a finite number of streams of finite width. Each stream has an individual point of minimum width where sonic conditions exist, shown as the transition between subsonic flow in blue and supersonic flow in yellow. These sonic points are distributed on a line distinct from the overall passage line of minimum width. The resulting minimum area line is shown in red along with the geometric minimum area line, to illustrate their disparity.

If this concept is extended to infinitesimal streamlines (and the flow is isentropic) each streamline will experience sonic conditions at its point of minimum area, coalescing to form the 2-dimensional sonic line. The effective throat area of a 2-dimensional nozzle is thus the sum of its streamlines' throat areas. This is distinct from the sonic line length, and may be expressed by the integral

$$A_{eff} = \int_1^2 \hat{\boldsymbol{v}} \cdot \hat{\boldsymbol{r}} \, dL \tag{2.1}$$

where $\hat{\boldsymbol{v}}$ is the unit vector of local flow velocity, $\hat{\boldsymbol{r}}$ is the unit vector perpendicular to the local sonic line, and the integral is performed on the scalar infinitessimal dL over the length of the sonic line, as illustrated in Figure 2.1b.

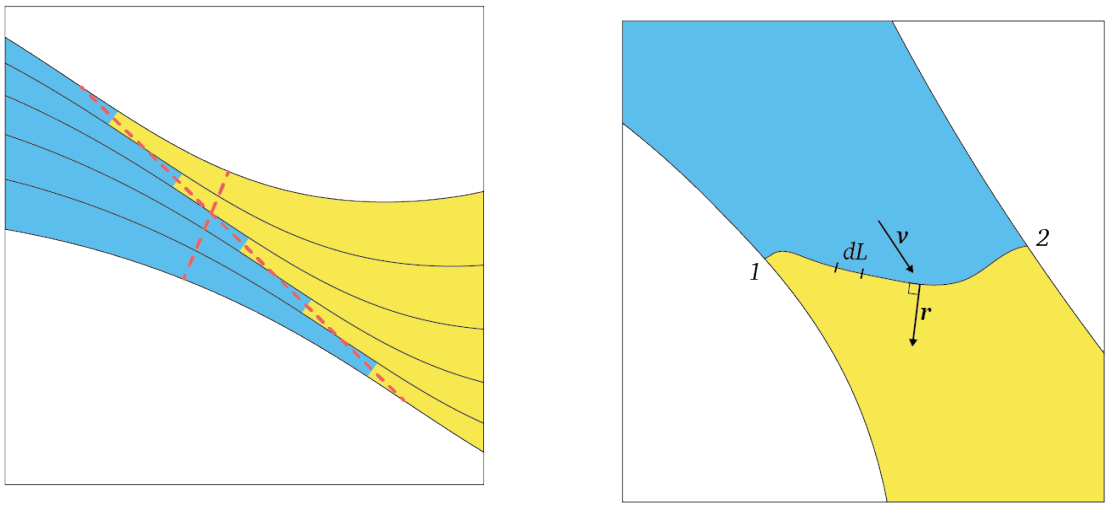

(a) Different minimum area points of dissimilar streams

(b) Integral for 2D nozzle equivalent throat area

Figure 2.1: Considerations for defining minimum area

In the case of 1-dimensional nozzle flow, Equation 2.1 collapses to the value of the throat area. In the case of 2D flow through an arbitrarily shaped nozzle such as a gas turbine nozzle guide vane, the integral describes the infinitesimal sum of the areas encountered by each streamline at the point of sonic conditions. It is proposed as a physically sensible 2D extension of the 1D concept of throat area, as opposed to placing a ruler across the narrowest point of passage to obtain a geometric throat area.

The present study will nonetheless discuss the reasons for which geometric throat area remains a useful predictor of NGV flow capacity in many cases, as has been noted in the literature. Deepak Thirumurthy et al [2] discussed the challenges and uncertainties associated with the accurate matching of an aeroderivative gas generation turbine. The authors' focus was on various means of predicting capacity to facilitate proper matching.

The authors noted that "the throat area of any blade or vane row has a strong influence on the overall capacity of the turbine. The vane or blade throat plane...is defined as the plane formed by the smallest passage area normal to the flow path. The effects are of first order when the throat area is changed for the first stage of the turbine."

2.1 1D vs 2D capacity uncertainty

The immediate challenge in quantifying 2D nozzle flow capacity is that analytical approaches are incomplete. If any nozzle's A_{eff} could be inferred from its geometry, it would be possible to investigate the effects of the geometry on the flow capacity to a high degree of accuracy, but the only way to find A_{eff} is to solve the flow computationally to obtain the $M = 1$ line. Once a CFD solution has been obtained, the flow capacity is predicted anyway.

Those concerned with mapping NGV geometry onto flow capacity are thus presented with 2 options: either perform CFD on every conceivable shape of NGV and create a lookup table of arbitrary fidelity, or analyse a relatively small set of CFD solutions to create heuristics about what types of geometric

changes cause what types of changes to the shape of the $M = 1$ line and local flow vectors.

Rolls-Royce plc have provided the present study with a family of NGV geometries suitable for such an approach, all from the Trent 900 engine. Geometric variation among Trent 900 NGVs has been subject to extensive measurement by Rolls-Royce. In one such set of studies, Terry Hall [3] and Giulio Zamboni [4] provided geometric definitions of 6 NGVs. These studies considered 2 slightly different production standards within the Trent 900 NGV family, which are referred to by the company as the M-skew standard and the EP1 standard.

Rolls-Royce randomly selected three production NGVs from each standard and measured their surface geometries using the *white light/GOM* scanning method. This resulted in the geometric definition files which were provided to the present study by Hall and Zamboni. These files do not include film cooling holes or the trailing edge slot. The trailing edges are smoothly rounded.

Significant variations exist among the geometry of the 6 NGVs, even when cooling features are not accounted for. Zamboni described the process for quantifying these variations in 3D, which will be discussed in Section 2.2. The present study defined an approach for deriving 2D geometries from the 3D files and quantifying the variations among them.

The 3D NGV surface shape was provided by Rolls-Royce as a set of co-ordinates which define 21 closed loops on the vane surface. Each loop consists of a pair of streamlines which diverge from a stagnation point on the vane's leading edge and converge at the trailing edge. The 11th loop was thus considered to be the closest approximation to a mid-span slice of the NGV.

MATLAB was used to process the 3D curve of the 11th loop, producing a 2D section via the following process.

1. Project the loop's coordinates onto a cylindrical surface whose radius is equal to the NGV annular radius at mid-span.
2. Periodically repeat the resulting shape in the circumferential direction to create an annulus of 2D vanes wrapped around the cylinder.
3. Transform the annulus into an infinite 2D linear cascade by taking the circumferential coordinate to be a vertical coordinate.

This process is illustrated in Figure 2.2.

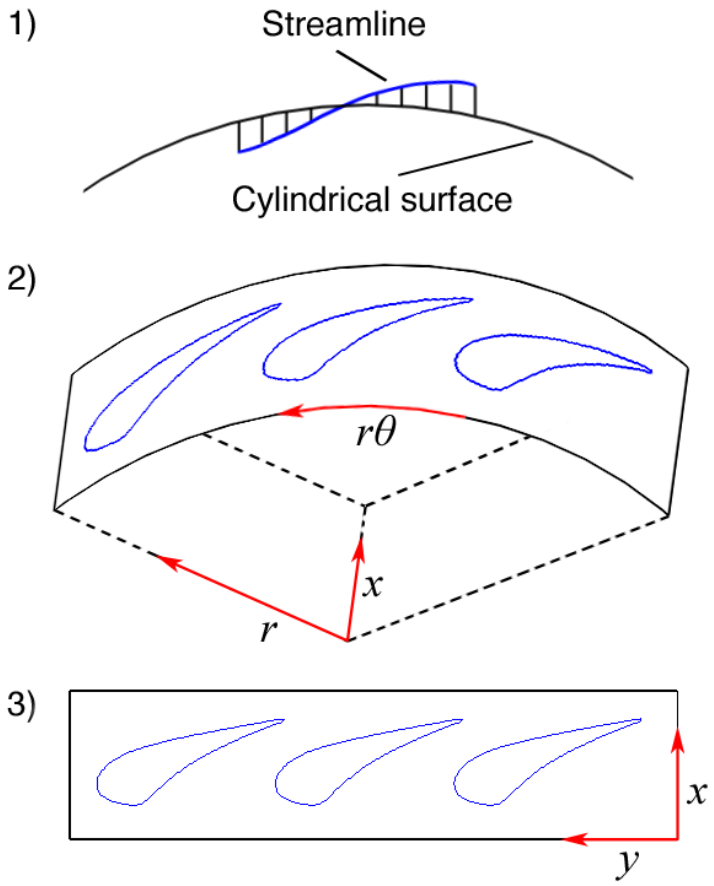

Figure 2.2: Creation of 2D mid-span approximation of NGV geometry

The resulting coordinates were connected to form a closed body. This body was placed in a computational domain consisting of a straight inlet section, a curved turning section, and a straight outlet section inclined at the NGV turning angle. The domain was modelled in Ansys Fluent, where the inlet boundary was specified to have total pressure p_{01} and the outlet was specified to have static pressure p_2. The remaining domain boundaries were made periodic with one another to preserve the 2D linear cascade. The NGV surface boundary was specified as a solid wall with a no-slip boundary condition and no heat conduction. The resulting computational domain is illustrated in Figure 2.3.

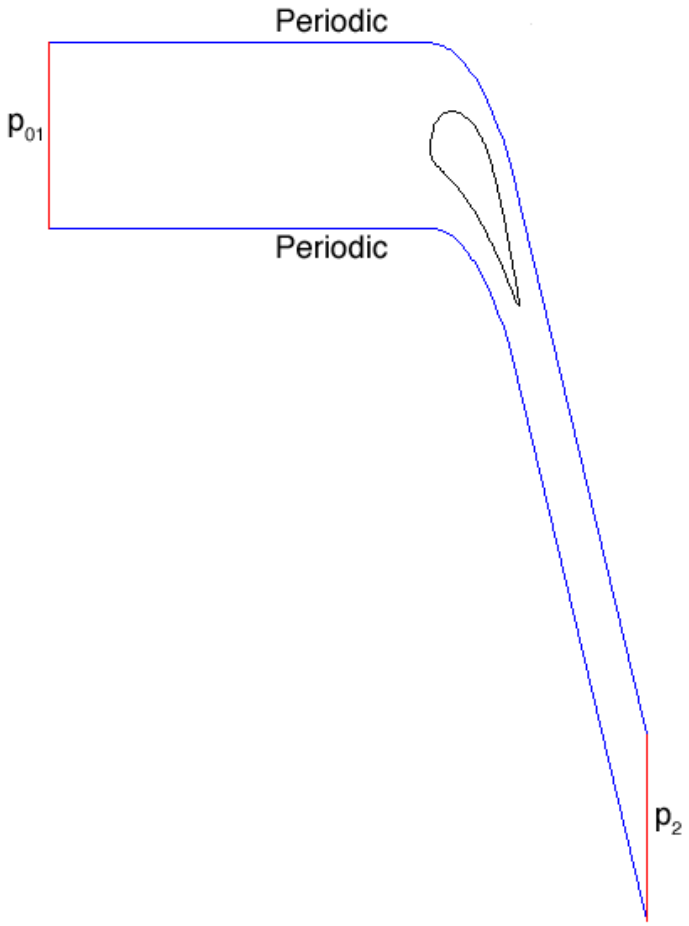

Figure 2.3: Computational domain and boundaries

This configuration has been the basis for all other 2D CFD analyses in the present study, where additional boundaries are added to account for cooling features as required. Values for the simulation were set according to Table 2.1.

Table 2.1: Boundary conditions at design pressure ratio for multi-vane capacity study

Parameter	Value
NGV series	Rolls-Royce Trent 900
NGV turning (degrees)	76.89
Design pressure ratio	1.79
Inlet total pressure (Pa)	4.33×10^6
Inlet total temperature (K)	300
Outlet static pressure (design) (Pa)	2.42×10^6
Outlet static temperature (Pa)	300
Solver type	Density-based
Cell count	35,000

For turbomachinery flows of this type, the boundary layer thickness will be shown to be large enough to significantly affect the NGV throat area. The mesh must resolve the whole boundary layer within a

region of high resolution which is sufficiently large to cover the maximum boundary layer thickness. The maximum thickness of a turbulent boundary layer is approximated by the formula

$$\delta \approx 0.37 \frac{L}{Re^{\frac{1}{5}}} \tag{2.2}$$

where L is the characteristic length in the direction of the flow (the approximate NGV chord length) and Re is the Reynolds number. The Reynolds number is defined as

$$Re = \frac{uL\rho}{\mu} \tag{2.3}$$

where u is a representative value for flow velocity and μ is the dynamic viscosity of the fluid within the temperature range of the flow. For compressible flow, the velocity and denisity are substituted to give

$$Re = \frac{M\sqrt{\gamma RT}L\frac{p}{RT}}{\mu} \tag{2.4}$$

which simplifies to

$$Re = \frac{L}{\mu}\sqrt{\frac{\gamma}{R}}\frac{p}{\sqrt{T}}M \tag{2.5}$$

$$Re = \frac{L}{\mu}\sqrt{\frac{\gamma}{R}}\frac{p_0}{\sqrt{T_0}}M\frac{\left(1+\frac{\gamma-1}{2}M^2\right)^{-\frac{\gamma}{\gamma-1}}}{\sqrt{\left(1+\frac{\gamma-1}{2}M^2\right)^{-1}}} \tag{2.6}$$

$$Re = \frac{L}{\mu}\sqrt{\frac{\gamma}{R}}\frac{p_0}{\sqrt{T_0}}M\left(1+\frac{\gamma-1}{2}M^2\right)^{\frac{\gamma+1}{2(1-\gamma)}} \tag{2.7}$$

Equation 2.7 was used to compute a Reynolds number for the case of choked or near-choked NGV flow with the following values, based on the values specified in Table 2.1.

Table 2.2: Values for calculating NGV Reynolds number

Parameter	Value
L	0.1 m
μ	18.45×10^{-6} Pas
p_0	4.33×10^6 Pa
T_0	300 K
γ	1.4
R	287 $\text{Jkg}^{-1}\text{K}^{-1}$
M	1

This resulted in a value of $Re = 5.5 \times 10^7$. Maximum boundary layer thickness was thus estimated using equation 2.2 to be 1 mm. This is of the order of 5% of the NGV throat width, so full resolution of the boundary layer is required for any CFD study of the effects of NGV geometric changes.

The NGV surface was enclosed in a structured quadrilateral mesh which extended out by 3 mm. Compared to the estimated maximum boundary layer thickness, the factor of 3 ensured that the whole boundary layer was captured, reduced the gradient of cell size change within the boundary layer mesh, and provided additional resolution within the base region downstream of the trailing edge, where boundary layer separation and entropy generation occur amid high surface curvature.

Full resolution of the boundary layer required placement of mesh elements within the laminar sub-layer. Regions within the boundary layer were assumed to be divided according to the *universal law of the wall*. This boundary layer model is derived from experimental measurements and dimensional analysis performed by Johann Nikuradse [5]. The author's motivation was the need to predict the velocity profile and thickness of turbulent boundary layers, given the free-stream conditions. The work is of renewed importance in the context of contemporary CFD such as the present study, where knowledge of appropriate boundary layer mesh resolution is mandatory.

Nikuradse showed that turbulent boundary layers in general exhibit a high degree of dimensional similarity if distance from the wall y is appropriately non-dimensionalised. The assumption was that qualitatively distinct regions of the boundary layer may be characterised by a dimensionless number that takes the place of y. Regions closer to the wall are expected to be dominated by viscous forces, and regions closer to the free-stream are expected to be dominated by inertial forces. The dimensionless wall distance parameter is thus expected to take similar form to the Reynolds number. It is defined as

$$y_+ = \frac{u_f y \rho}{\mu} \tag{2.8}$$

where u_f is the friction velocity, defined as

$$u_f = \sqrt{\frac{\tau_w}{\rho}} \tag{2.9}$$

where τ_w is the shear stress at the wall boundary. Equation 2.9 thus characterises the wall shear stress as a velocity which is used in the Reynolds-type formulation of Equation 2.8. τ_w is defined as

$$\tau_w = \frac{1}{2} C_f \rho u^2 \tag{2.10}$$

where C_f is a coefficient of skin friction and u is the free-stream velocity. C_f may be computed from the free-stream Reynolds number according to the correlation proposed by Hermann Schlichting [6]

$$C_f = \left(2\log_{10} Re - 0.65\right)^{-2.3} \tag{2.11}$$

For compressible flows, equation 2.10 may be expressed as

$$\tau_w = \frac{1}{2} C_f \frac{p}{RT} M^2 \gamma R T \tag{2.12}$$

$$\tau_w = \frac{1}{2} C_f \gamma p_0 M^2 \left(1 + \frac{\gamma - 1}{2} M^2\right)^{-\frac{\gamma}{\gamma - 1}} \tag{2.13}$$

allowing a compressible expression of u_f as

$$u_f = \sqrt{\frac{\frac{1}{2} C_f \gamma p_0 M^2 \left(1 + \frac{\gamma-1}{2} M^2\right)^{-\frac{\gamma}{\gamma-1}}}{\rho_0 \left(1 + \frac{\gamma-1}{2} M^2\right)^{-\frac{1}{\gamma-1}}}} \tag{2.14}$$

$$u_f = \sqrt{\frac{C_f \gamma R T_0 M^2}{2 + (\gamma - 1) M^2}} \tag{2.15}$$

and allowing a compressible expression of y_+ as

$$y_+ = \sqrt{\frac{C_f \gamma R T_0 M^2}{2 + (\gamma - 1) M^2}} \frac{y}{\mu} \frac{p_0}{R T_0} \left(1 + \frac{\gamma - 1}{2} M^2\right)^{-\frac{\gamma}{\gamma - 1}} \tag{2.16}$$

$$y_+ = \frac{y}{\mu}\sqrt{\frac{\gamma}{R}}\frac{p_0}{\sqrt{T_0}}\sqrt{\frac{C_f}{2}}M\left(1+\frac{\gamma-1}{2}M^2\right)^{\frac{\gamma+1}{2(1-\gamma)}} \tag{2.17}$$

This expression is of similar form to the expression for Reynolds number in equation 2.7. Both are shown to be a function of Mach number and of the upstream conditions $\frac{p_0}{\sqrt{T_0}}$. If these expressions are normalised against the upstream conditions in a similar way to flow capacity, it is shown that both the dimensionless speed *Re* and the dimensionless boundary layer thickness y_+ are purely functions of Mach number and of a geometric parameter - L and y respectively. This is subject to the assumptions that μ is approximately constant within the range of temperatures and $\sqrt{\frac{C_f}{2}}$ is approximately constant for sufficiently high Reynolds numbers.

Equation 2.17 may be rearranged to compute a real distance y from the wall given a value of y_+. In the general case of turbulent boundary layers, the laminar sublayer occupies the region of $y_+ < 5$. The present study placed the first layer of mesh nodes at a wall distance corresponding to a y_+ value of 2.5. This is in accordance with a study of laminar sublayer resolution by Salim M. Salim and Siew-Cheong Cheah [7].

Within the structured boundary mesh, element size was grown so that the outermost elements had an aspect ratio of approximately $\frac{1}{2}$. Beyond this, the domain was populated with an unstructured quadrilateral-dominant mesh. Node distributions along the two periodic boundaries were made identical, and nodes adjacent to the structured boundary layer mesh were made to match its outermost node distributions. Within the general domain, unstructured mesh generation was automated using Ansys Fluent's built-in meshing feature.

Put more mesh pictures here.

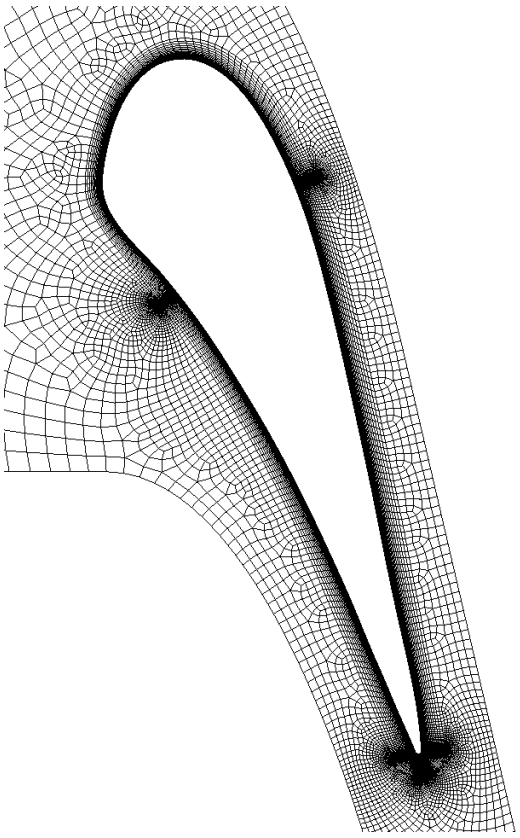

Figure 2.4: Mesh for Trent 900 smooth-vane capacity study

When the "throat area" of the 2D family is plotted against their capacity at a choking PR, it shows a pretty good proportional relationship. This is despite some obvious differences in the shape of the M1 line.

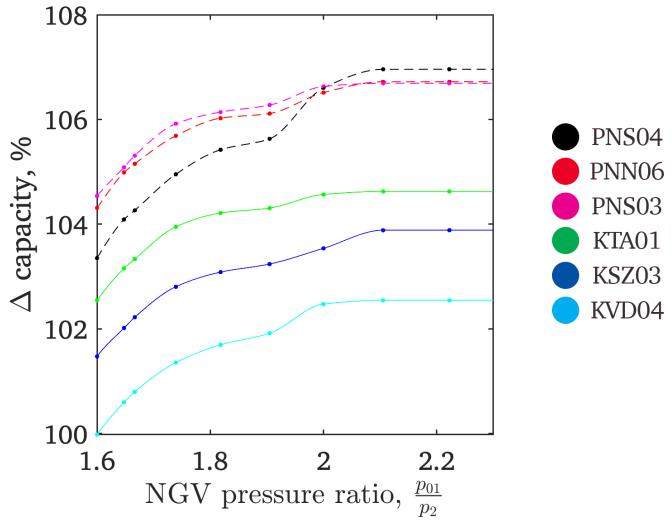

Figure 2.5: 2D capacity trends for 6 Trent 900 NGVs

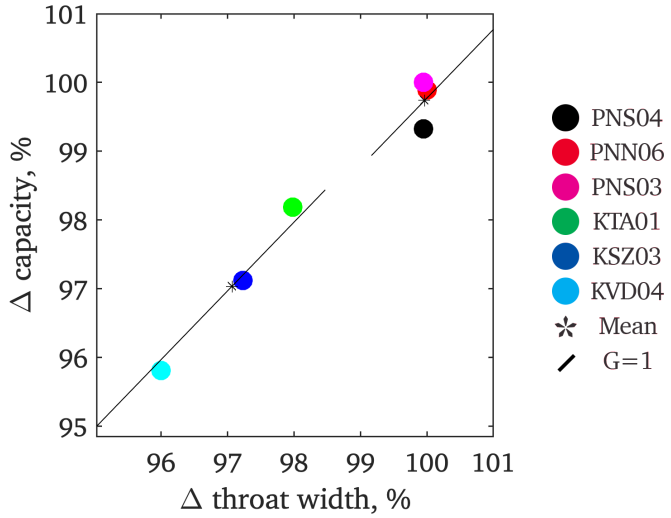

Figure 2.6: 2D NGV capacity percentage delta as a function of 2D throat width for 6 vanes

Why are there still small deviations? That is, can I present a better definition of throat area that fits even better? Possible topics:

Most likely it will follow the 1D rule if it is taken to be that streamline's M1 point. But not certain.

the relationship between the minA line and the M1 line

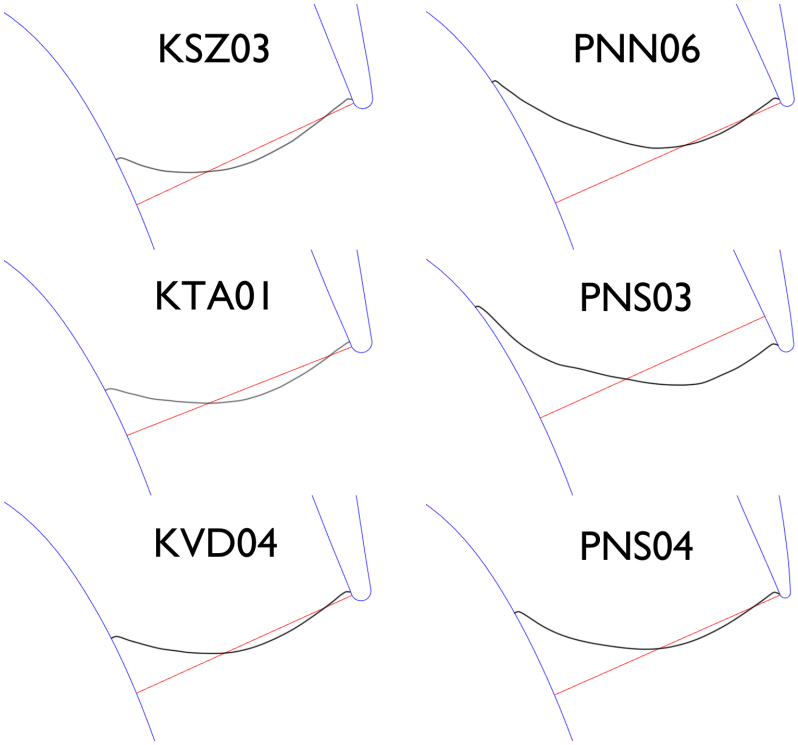

Figure 2.7: Sonic lines for 6 Trent 900 NGVs

the total length of each M1 line

a plot of capacity vs M1 line length

Why aren't there larger deviations? That is, can I derive a sensible geometric parameter and show that it isn't changing significantly?

Is this all really at design PR? What if the M1 lines were obtained at more choked PRs but I forgot to say so? What does the correlation look like at other PRs?

2.2 2D vs 3D capacity uncertainty

Zamboni defined the Rolls-Royce process for calculating 3D throat area as follows: "Along each vane span section, the throat line is defined as that line which connects the TE of one vane with the point of minimum distance on the suction surface of the nearby vane in the tangential direction. For a vane with TE slot, the TE point is defined as the start of the cut back... The throat surface interpolates all the throat lines spanwise."

3D CFD data was shared by Rolls-Royce for comparison with the 2D data. The point is to see why 3D is still so different from 2D, ie what are we failing so badly to predict with 2D?

Discuss the most important ways in which the 3D capacity trends are different from the 2D ones. From a superficial look it appears that the 3D trends never choke. What could this mean about their having a M1 line at all?

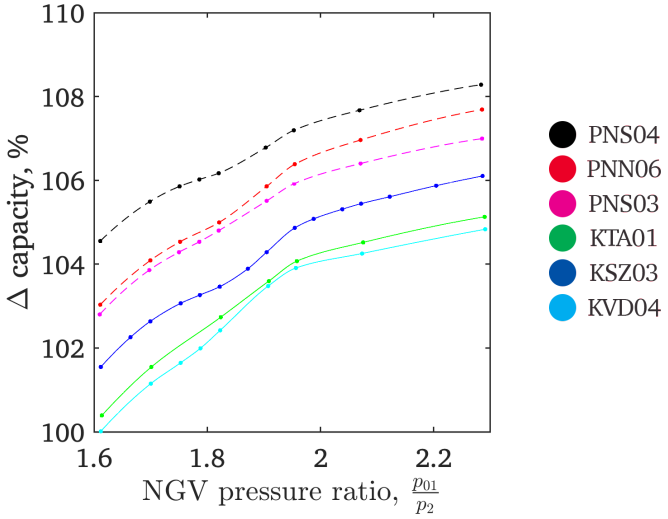

Figure 2.8: 3D capacity trends for 6 Trent 900 NGVs

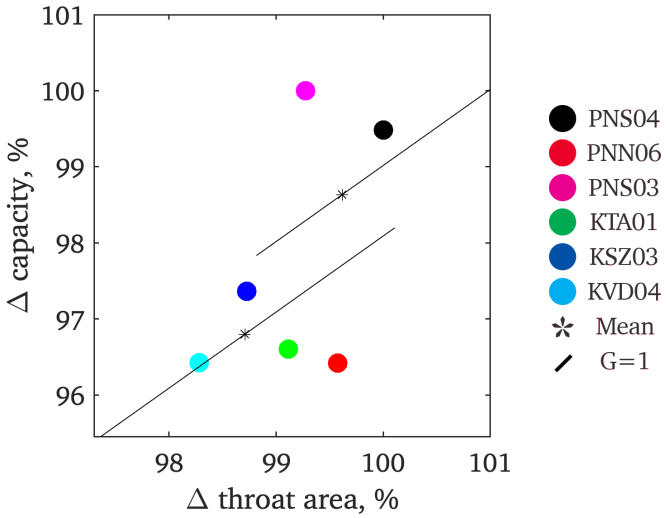

Figure 2.9: 3D NGV capacity percentage delta as a function of 3D throat area for 6 vanes

What does the correlation look like at other PRs?

Review 3D effects from the literature.

Chapter 3

Trailing edge

3.1 Definitions of loss for trailing edge performance evaluation

Loss may refer to any process whereby the recoverable energy of a turbomachinery flow is reduced during transit through a turbine stage, other than by shaft work, with corresponding entropy creation. Minimisation of loss remains a primary obective of turbomachinery design, but there is not a universal consensus on how to quantify it.

Daniel Back da Trinidade et al [8] characterised sources of loss as shock loss, profile losses, tip leakage, endwall losses, and cooling losses. Tip leakage results from flow through the clearance space between the vane tips and the casing. It will not be considered by the present study, since the present study is of fixed NGVs. Endwall losses result from 3-dimensional secondary flows, and will not be considered in the present study which is of 2-dimensional phenomena.

Trinidade et al characterised shock loss as resulting from entropy creation across the shock wave during supersonic flow. The present study will consider this mechanism during discussion of CFD results at choking pressure ratios.

Profile loss was characterised by entropy creation by viscosity in the boundary layer on the blade surface. Entropy generated near the blade's trailing edge was considered as profile loss due to the high entropy creation in the wake region following flow separation at the trailing edge. The authors extended this definition to include the entropy generated as the flow turns tightly around the trailing edge curvature and forms expansion waves.

The authors also defined the category of cooling losses to refer to the aerodynamic penalties incurred by cooling in general, namely "thicker blade profiles from coolant holes, interaction of coolant film with the blade boundary layer, mixing losses between coolant and main flow and endwall losses." The present study seeks to isolate the mechanisms whereby film cooling causes boundary layer changes and mixing effects, discussing film cooling in Chapter 4.

The present study seeks to define a coefficient of NGV total pressure loss whose arguments are flow measurements or numerically predicted parameters. Giel et al surveyed the total pressure wake profiles of a blade at mid-span, defining a *total pressure coefficient* as

$$Cp_t = \frac{p_{01} - p_{02}}{p_{01} - p_2} \tag{3.1}$$

where p_{01} and p_{02} are the inlet and wake total pressures, and p_2 is the wake static pressure. This

definition is to be used for the total pressure wake profiles in this thesis. The authors also defined a *kinetic energy loss coefficient* as

$$e_2 = \frac{\left(\frac{p_{01}}{p_{02}}\right)^{\frac{\gamma-1}{\gamma}} - 1}{\left(\frac{p_{01}}{p_2}\right)^{\frac{\gamma-1}{\gamma}} - 1} \tag{3.2}$$

Giel et al's results will be compared to those of this study, considering wake profiles and loss as a function of trailing edge thickness.

Jie Gao et al [9] defined a slightly different *total pressure loss coefficient* as

$$C_p t = \frac{p_{01} - p_{02}}{p_{02} - p_2} \tag{3.3}$$

Discuss these two slightly different definitions.

Saha paper has its own loss definitions too - seems to be doing a definition that considers the coolant/mainstream mass flow ratio.

$$\zeta = 1 - \frac{(1+Y)\left(1 - \left(\frac{p_2}{p_{02}}\right)^{\frac{\gamma-1}{\gamma}}\right)}{\left(1 - \left(\frac{p_2}{p_{01}}\right)^{\frac{\gamma-1}{\gamma}}\right) + Y\left(1 - \left(\frac{p_2}{p_{0c}}\right)^{\frac{\gamma-1}{\gamma}}\right)} \tag{3.4}$$

where Y is the coolant-to-mainstream mass flux ratio.

In the case of no coolant flow this becomes

$$\zeta = 1 - \frac{1 - \left(\frac{p_2}{p_{02}}\right)^{\frac{\gamma-1}{\gamma}}}{1 - \left(\frac{p_2}{p_{01}}\right)^{\frac{\gamma-1}{\gamma}}} \tag{3.5}$$

3.2 Effects of trailing edge shape uncertainty on capacity predictability

If nozzle guide vane flow capacity is known to be a function of effective throat area, we must survey the practical reasons for which effective throat area might vary. In a real engine, NGV effective throat area might depart from its design value if the NGVs depart from their design shape, either because of the finite precision of manufacturing, or because of erosion while in service.

A goal of the present study is to help ascertain how much these off-design conditions might limit the predictability of NGV flow capacity, and to comment on ways to mitigate this limitation. The NGV trailing edge is an area of focus because it is particularly succeptible to both finite-precision and in-service departures from its design shape.

The trailing edge is succeptible to finite-precision departures from its design shape because of how it is manufactured. Vane pairs are cast to a finite precision as discussed in Section 2.1, where significant geometric variation appears in vanes even without cooling features. The vanes are then subject to machining to finish off the trailing edge shape. The finishing creates the most aerodynamic trailing edge possible, with a thin suction-side flange that cleanly meets the endwalls, and a flange chord

length that is consistent across the span of the trailing edge. The creation of a repeatable minimum geometric area cannot be said to be a primary objective.

The trailing edge is succeptible to in-service departures from its design shape because it is the most fragile part of the vane. The NGV remains largely intact over a lifetime of extremely hot supersonic flow, but the trailing edge flange may be subject to significant erosion. If there is a blockage in any of the plena which feed the trailing edge slot, part of its span will receive reduced coolant flow, accelerating the degradation of the trailing edge flange near that area. Such cooling failures are not uncommon in sandy environments.

This study will consider the potential worst case for in-service erosion of the suction-side flange, namely its complete deletion. This worst-case erosion is assumed to take place at the NGV mid-span because this area is exposed to the greatest flow speeds and temperatures. This justifies 2-dimensional simulation of the mid-span flow. The goal is to parameterise changes to the flange and comment on how these changes alter the effective minimum area and the NGV flow capacity.

2D CFD has been used to model the effects of incremental removal of material from the trailing-edge suction-side flange of an NGV.

Present boundary conditions.

Geometry made by Fig 2.2

Domain is Fig 2.3

BCs are:

Table 3.1: Boundary conditions for trailing edge suction-side flange shape uncertainty study

Parameter	Value
NGV series	Rolls-Royce Trent 900
NGV turning (degrees)	76.89
Design pressure ratio	1.79
Inlet total pressure (Pa)	4.33×10^6
Inlet total temperature (K)	300
Outlet static pressure (design) (Pa)	2.42×10^6
Outlet static temperature (Pa)	300
Solver type	Density-based
Cell count	35,000

Present mesh with larger and better pictures, and show how the mesh is altered as erosion amount varies. Plan of action - figure out how to save a specific viewpoint in Fluent, and how to take good pictures. Make sure this viewpoint is suitable for both the SS and PS pictures.

Show capacity trend for all the data as an initial summary, then show capacity vs erosion amount for a couple of relevant PRs (perhaps design and fully choked)

2D CFD predicts a maximum 2 percent change in capacity (when the flange is completely gone)

What is changing in the flow as a result of the erosion, and is it driving capacity change via the expected route of throat area changes (whatever we've decided is the best definition of throat area

in the previous chapter)

Cite the state of the art for measuring the capacity of a ring of real parts - Burdett: Daniel Burdett - Analysis of ultra-low uncertainty gas turbine flow capacity measurement techniques [10] Arguing: Experimental capacity measurement of a ring of NGVs is now excellent and getting better. CFD still has trouble with small geometric changes because they are so tiny compared with even small deviations in the mesh. The TE is especially difficult to model with CFD because it involves so many different flows meeting and mixing, with unpredictable geometry Raw data: Experimental data showing continued improvements to the accuracy of the unsteady capacity measurement technique I discuss: The TE is indeed particularly hard to predict. Having established an extremely accurate measurement technique for an annulus of NGVs, how could such ideas be adapted to focussing on small geometric changes at the TE? I also cite: The history of this technique at Oxford, showing it has embodied a continual evolution in measurement accuracy and sensitivity to boundary conditions, but has been relatively underused for the study of geometric effects

Jie Gao - Experimental and numerical investigations of trailing edge injection in a transonic turbine cascade [9] Arguing: TE coolant ejection is good for reducing the wake size and reducing shock effects on the exit angle Raw data: Their experimental and CFD linear cascade, five-hole probe data and surface pressure plots, downstream loss profile I discuss: Does it match my blowing rate study? Do my turning angles agree with theirs as Mach number changes? Do I see the same reduction of shocks? Do I broadly agree about the benefits of TE ejection? Remember badly-predicted turning angles are like bad capacity predictions I also cite: Whoever's loss definition they use - why didn't they compare it to others? My raw data: A lot of my own TE CFD

Gao et al experimentally and numerically investigated the external flow field near the trailing edge of a linear cascade with trailing edge injection. The authors' focus was on the effects of the trailing edge coolant flow on the vane's loss mechanisms and flow exit angle. Without trailing edge injection, increased exit isentropic Mach number caused the appearance of trailing edge suction side shock waves which altered the flow angle. With trailing edge injection, there was a slight reduction in this shock effect but a strong reduction in the shock wave near the trailing edge pressure side.

3.3 Performance of an alternative trailing edge design

Improved materials and manufacturing techniques may neccessitate alternative trailing edge geometries. Paul W. Giel et al [11] noted that "in the pursuit of higher turbine inlet temperatures for reduced fuel burn and emissions consistent with NASA's goals [12], Ceramic Matrix Composite (CMC) materials are now being implemented in gas turbine engines...They enable higher turbine inlet temperatures, thus enabling higher overall pressure ratios (OPRs) for the engine and higher thermal efficiency."

The authors used a linear cascade to measure the aerodynamic performance of a set of blades representing the geometric constraints of the CMC manufacturing method. Of main concern was the constraint that "the trailing edge thicknesses of CMC blades are anticipated to be significantly larger than those of current state-of-the-art metallic blades," which may be expected to cause increased loss.

Discuss other justifications for studying this design - is it more predictable because it suffers less erosion?

Introduce my alternative design: 2D CFD was done on an alternative design of TE featuring centred

coolant ejection. This shape of TE was also incrementally cut back on the pressure side so as to more resemble the existing TE design.

Present boundary conditions.

Table 3.2: Boundary conditions for trailing edge centred-ejection design study

Parameter	Value
NGV series	Rolls-Royce Trent 900
NGV turning (degrees)	76.89
Design pressure ratio	1.79
Inlet total pressure (Pa)	4.33×10^6
Inlet total temperature (K)	300
Outlet static pressure (design) (Pa)	2.42×10^6
Outlet static temperature (Pa)	300
Solver type	Density-based
Cell count	35,000

Present mesh with larger and better pictures, and show how the mesh is altered as the design is altered.

Plot capacity trends for the centred-ejection designs vs the baseline.

Is there better capacity predictability because the effects of erosion are less pronounced due to the thicker flanges?

Discuss whether this loss may be worse or better if a centred-ejection design is used, still perhaps plotting more than one definition of loss.

When using this configuration, is there an optimal blowing rate that might re-energise the base region? Plot blowing rate vs loss, remembering that the graph I currently have is erroneously for the other type of TE, not for the centred-ejection kind. Should I try to re-run just this one thing?

Compare my centred-ejection TE with a "naturally-formed by erosion" centred-ejection TE from the literature.

To be filed:

Ranjan Saha - SHOWER HEAD AND TRAILING EDGE COOLING INFLUENCE ON TRANSONIC VANE AERO PERFORMANCE [13] Arguing: Loss turns out very differently depending on which loss equation you use, and some formulations might be better than others. Raw data: Their annular sector rig which tested NGVs with and without showerhead and TE coolant to quantify loss. I discuss: How do their definitions of loss compare to mine and others', and is there an answer to which one is best in general? I also cite: All the other possible loss definitions, going back to Raffel and Kost and further if necessary. My raw data: Any of my CFD data can yield loss according to any preferred definition, but this is most pertinent to my T900 TE cutbacks discussion.

Chapter 4

Leading edge

It is sometimes necessary to add extra cooling holes on the suction-side at the LE.

Coolant introduced into this part of the flow has complex interactions with the mainstream, affecting NGV capacity.

4.1 sensitivity of capacity to cooling holes on the leading suction side

Adding cooling holes causes complex effects - here discussed as loss, so I need citations for capacity too: Jie Gao - Experimental and numerical investigations of hole injection on the suction side throat of transonic turbine vanes in a cascade with trailing edge injection [14] Arguing: Like their above paper but with a SS cooling slot. It causes passage blockage, a thicker wake, and more loss. But when there are shock waves, the film coolant enhances the TE PS shock but reduces the TE SS shock, which could be used toreatly reduce the TE SS shock if the injection is upstream of the throat Raw data: Their experimental and CFD linear cascade, with strong emphasis placed on the loss definitions and techniques established by Denton and Xu, Mee et al, and Schobieri I discuss: Ways in which my SS injection might interact with the flow (including shockwaves) as they suggest. Will I see it without having TE injection too? I also cite: Denton and Xu, Mee et al, and Schobieri for established precident on loss quantification My raw data: My moving coolant row study

2D CFD was done on an XWB NGV with no coolant features apart from the addition of a single cooling row on the upstream suction side. The position of this featrure was varied, thus varying whereabouts in the flow the coolant was introduced.

Present boundary conditions.

Table 4.1: Boundary conditions for suction-side cooling hole position study

Parameter	Value
NGV series	Rolls-Royce Trent XWB 84K
NGV turning (degrees)	73.97
NGV throat width (m)	$1.25 \times 10^{-}2$
Design pressure ratio	1.65
Inlet total pressure (Pa)	4.33×10^{6}
Inlet total temperature (K)	300
Outlet static pressure (Pa)	2.63×10^{6}
Outlet static temperature (Pa)	300
Coolant/mainstream mass flow ratio	0.003
Solver type	Density-based
Cell count	40,000

Present mesh, showing how the variable location coolant row is introduced.

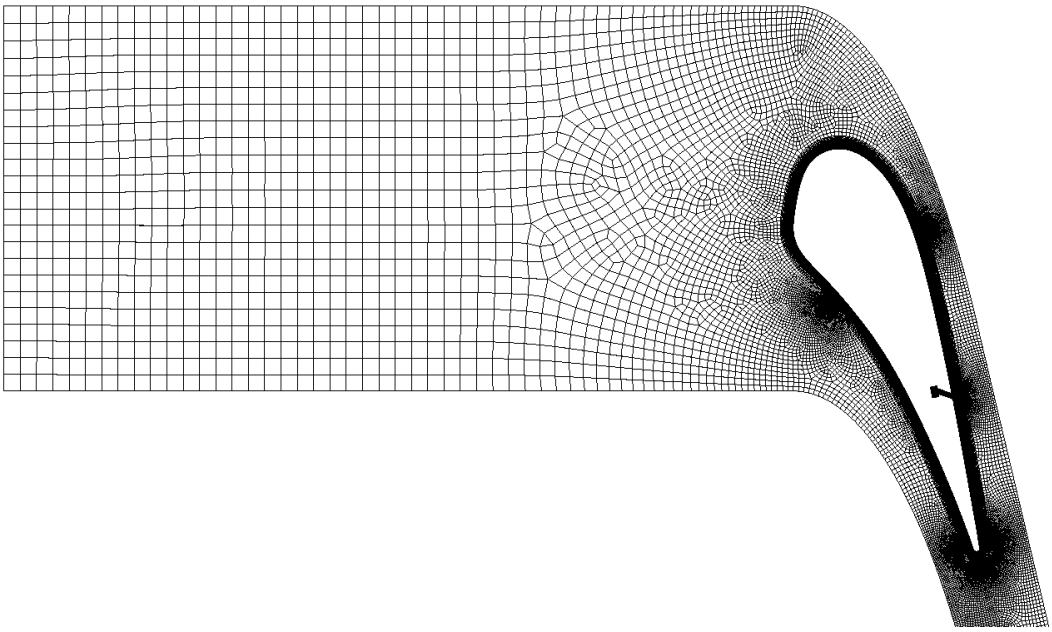

(a) XWB mesh for NGV and upstream domain

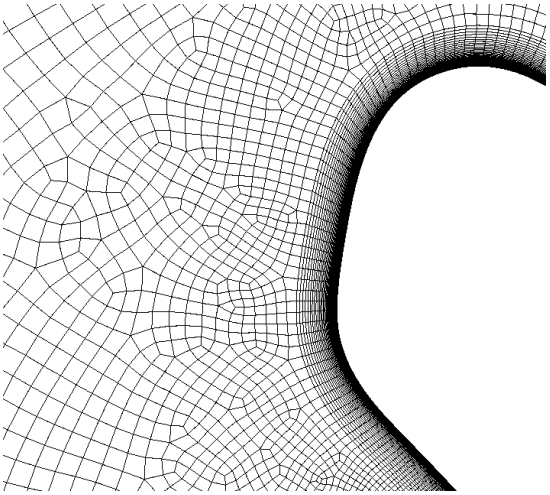

(b) XWB mesh for leading edge

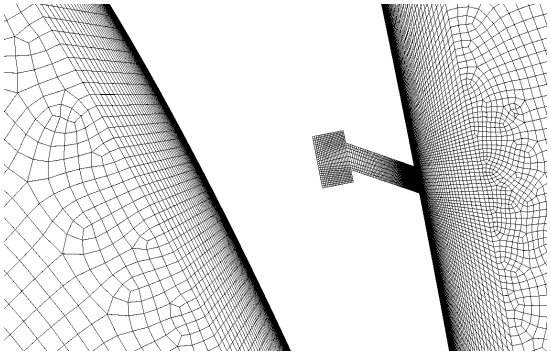

(c) XWB mesh for cooling hole and plenum

Figure 4.1: Details of mesh for XWB single cooling hole study

Review the literature for why correctly modelling turbulence is important for capturing the mainstream/coolant mixing, and thus why two turbulence models are compared.

Plot capacity changes versus hole position and discuss its causes, mentioning the literature reviewed in the chapter intro (plus the two definitions of capacity where coolant is concerned - which one is used in earlier chapters??) A maximum 0.5 percent change in capacity resulted from an unrealistically drastic shifting of a 2D cooling slot along the vane's suction side.

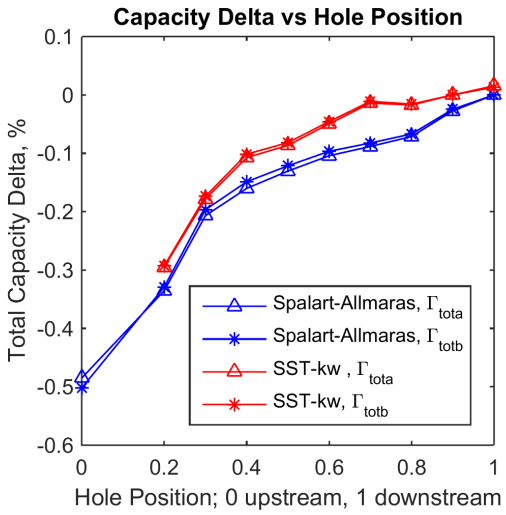

Figure 4.2: Total capacity percentage delta as a function of single cooling hole position

Things that might be driving the change in capacity, and that can be examined from the existing data: Changing boundary layer thickness causing a change in effective throat area

4.2 Consideration of corrections necessary to interpret 2D result

Different:

Mass flow rate between a 2D slot and a 3D row of holes

Mixing between coolant and mainstream

Angle of ejection

Papers about matching the conditions when simulating a cooling row:

S. Ravelli - NUMERICAL ASSESSMENT OF DENSITY RATIO AND MAINSTREAM TURBULENCE EFFECTS ON LEADING EDGE FILM COOLING: HEAT AND MASS TRANSFER METHODS [15] Arguing: In a CFD simulation of four film cooling hole rows, the usual parameters (DR, BR, MFR, TuI) aren't enough to ensure you have matched the engine conditions Raw data: A previous experimental study (PSP) to validate their CFD, and their CFD I discuss: Criticise my own signle cooling slot work - is it really representative enough for its capacity effects to be predictable I also cite: Other CFD on film cooling My raw data: My single cooling row data, emphasis on the CFD parameters and setup

Giovanna Barigozzi - Experimental investigation of the interaction between showerhead coolant jets and main flow [16] Arguing: When film coolant is ejected upstream , observed high turbulence and velocity fluctuations suggest the mixing is a random process without coherent structures, and unsteady, and 3D Raw data: Their experimental study, including pressure-sensitive paint and particle-image velocimetry I discuss: Do we know less than we thought about how much film coolant is actually getting to the LE SS? Reason why you might want an extra row there? Also, clear support for my arguing that proper CFD investigations of SS LE film cooling should not be a 2D slot and should not be steady

Wei He - Film cooling and aerodynamic performances of a turbine nozzle guide vane with trenched cooling holes [17] Arguing: A novel design for film cooling holes, using a zigzag-shaped trench, has some advantages but is only really suitable for the middle PS Raw data: Their 3D CFD on a single-vane linear cascade, where the trench moves around various positions I discuss: They mention BR etc, relevant to me. Their movable trench is a bit like my movable 2D slot, except it is mainly confined to the PS, whereas mine is on the SS. But my quasi-3D study could be easily adapted to repeat their study of the novel trench shape My raw data: My Q3D study

Bibliography

[1] A. Guiffre' and M. Pini, "Design guidelines for axial turbines operating with non-ideal compressible flows," *Proceedings of ASME Turbo Expo*, 2020.

[2] D. Thirumurthy, J. C. C. Coca, and K. Suraweera, "Capacity matching of aeroderivative gas generator with free power turbine: Challenges, uncertainties, and opportunities," *Proceedings of ASME Turbo Expo*, 2019.

[3] T. Hall, "Trent 900 CFD investigation of HPNGV capacity sensitivity to trailing edge geometry," Tech. Rep. DNS 170140, Rolls-Royce plc, Gipsy Patch Lane, Filton, Bristol, March 2011.

[4] G. Zamboni, "HYDRA CFD of the trent 900 EP1 turbine high pressure nozzle guide vane: analysis of the trailing edge slot geometry influence on capacity predictions using gom scanned data," Tech. Rep. DNS 181981, Rolls-Royce plc, Gipsy Patch Lane, Filton, Bristol, July 2012.

[5] J. Nikuradse, "Laws of flow in rough pipes," *VDI Verlag research booklet; "supplement to Research in the field of engineering"*, vol. 361, no. B4, 1933.

[6] H. Schlichting, *Boundary Layer Theory*. New York, NY, USA: McGraw-Hill, 1979.

[7] S. M. Salim and S.-C. Cheah, "Wall y+ strategy for dealing with wall-bounded turbulent flows," *Proceedings of the International MultiConference of Engineers and Computer Scientists*, vol. II, 2009.

[8] D. B. da Trinidade, P. Bugala, and D. Simone, "Review of loss models for high pressure turbines," *Journal of KONES Powertrain and Transport*, vol. 25, no. 2, pp. 37–44, 2018.

[9] J. Gau, M. Wei, W. Fu, Q. Zheng, and G. Yue, "Experimental and numerical investigations of trailing edge injection in a transonic turbine cascade," *Elsevier Journal of Aerospace Science and Technology*, vol. 92, pp. 258–268, 2019.

[10] D. Burdett, C. Hambidge, and T. Povey, "Analysis of ultra-low uncertainty gas turbine flow capacity measurement techniques," *IMechE Journal of Power and Energy*, vol. 0, no. 0, pp. 1–27, 2020.

[11] P. W. Giel, V. Shyam, P. Juangphanich, and J. P. Clark, "Effects of trailing edge thickness and blade loading distribution on the aerodynamic performance of simulated cmc turbine blades," *Proceedings of ASME Turbo Expo*, 2020.

[12] S. M. Jones, W. J. Haller, and M. T. Tong, "An n+3 technology level reference propulsion system," *NASA technical memorandum*, 2017.

[13] R. Saha, J. Fridh, and T. H. Fransson, "Shower head and trailing edge cooling influence on transonic vane aero performance," *Proceedings of ASME Turbo Expo*, 2014.

[14] J. Gau, M. Wei, Y. Liu, Q. Zheng, and P. Dong, "Experimental and numerical investigations of hole injection on the suction side throat of transonic turbine vanes in a cascade with trailing edge injection," *IMechE Journal of Aerospace Engineering*, vol. 232, no. 8, pp. 1454–1466, 2017.

[15] S. Ravelli, H. Abdeh, and G. Barigozzi, "Numerical assessment of density ratio and mainstream turbulence effects on leading edge film cooling: Heat and mass transfer methods," *Proceedings of ASME Turbo Expo*, 2020.

[16] G. Barigozzi, L. Casarsa, F. Pagnacco, and S. Rouina, "Experimental investigation of the interaction between showerhead coolant jets and main flow," *Elsevier Journal of Experimental Thermal and Fluid Science*, vol. 104, pp. 43–58, 2019.

[17] W. He, Q. Deng, W. Zhou, T. Gau, and Z. Feng, "Film cooling and aerodynamic performances of a turbine nozzle guide vane t with trenched cooling holes," *Elsevier Journal of Applied Thermal Engineering*, vol. 150, pp. 150–163, 2019.